Nonradiative Deexcitation Dynamics of 9H-Adenine: An OM2 Surface Hopping Study

E. Fabiano* and W. Thiel

Max-Planck-Institut für Kohlenforschung, Kaiser-Wilhelm-Platz 1, D-45470 Mülheim an der Ruhr, Germany

Received: April 17, 2008; Revised Manuscript Received: May 21, 2008

The nonradiative relaxation of 9H-adenine was studied at the semiempirical OM2/MR-CI level using the surface-hopping approach. Geometry optimizations of energy minima and conical intersections as well as single-point calculations of excitation energies at critical points were performed to characterize the relevant potential energy surfaces of 9H-adenine and to assess the accuracy of the OM2 results. Surface-hopping calculations were performed to describe the nonradiative dynamics of 9H-adenine after vertical excitation into the optically active state. They showed that the deexcitation process is mainly governed by a two-step relaxation consisting of an ultrashort component and a longer component. These findings compare well with experimental results from time-resolved photoelectron spectroscopy.

1. Introduction

The nucleic acid bases are the most important constituents of genetic material. For this reason, their electronic properties have been the subject of a large number of experimental and theoretical studies in recent years.[1–5] In particular, numerous investigations have addressed the photodynamical behavior of DNA and RNA bases to understand the origin of their photostability after UV irradiation. Photostability is, in fact, one of the most important properties of nucleobases. Nucleic acid bases absorb strongly in the 200−300 nm range and are potentially vulnerable to sun UV irradiation. The excess energy following photoexcitation could initiate photoreactions and lead to genetic mutations. However, DNA and RNA bases are extremely stable with respect to photodegradation as the excitation energy is efficiently dissipated through internal conversion and then transferred to the environment.

Adenine is often taken as a prototypical example of this behavior. It shows a broad absorption band with an onset at 275 nm (4.50 eV) and a maximum at 252 nm (4.92 eV).[1,6] On the basis of polarized absorption measurements and magnetic circular dichroism and circular dichroism experiments,[7–9] this band is assigned to two $\pi\pi^*$ states with similar energies. The two states, differing in relative intensity and direction of the transition moment, are usually labeled as L_a and L_b. A third state, of $n\pi^*$ character, is also found at similar energies. Its existence cannot be directly deduced from the absorption spectra; however, inspection of circular dichroism spectra reveals the presence of an $n\pi^*$ state hidden under the strong $\pi\pi^*$ peak and located 0.073 eV below the $\pi\pi^*$ state.[9]

Pump−probe experiments on jet-cooled adenine yielded a lifetime of 1.0 ps.[10,11] Subsequently, time-resolved spectra in the gas phase revealed a biexponential decay, involving a short component with a lifetime of 40−100 fs and a longer component with a lifetime between 750 fs and 1 ps.[12–17] The short timescales of these processes suggest that the electronic decay is due to intramolecular nonadiabatic phenomena involving the quasidegenerate low-lying singlet excited states and the ground state.

Computational studies have demonstrated the existence of at least three geometrical configurations connecting the excited states to the ground state via a conical intersection. The first, characterized by an out-of-plane ring deformation, is the conical intersection connecting the $\pi\pi^*$-L_a state and the ground state.[18–24] A second conical intersection links the $n\pi^*$ state with the ground state and is characterized by a strong out-of-plane deformation of the amino group.[18,20,22–24] Finally, crossings have been reported between the ground state and $\pi\sigma^*$ states due to out-of-plane deformation of the six-membered ring, hydrogen abstraction from the amino and azine groups, or opening of the five-membered ring.[18,25,26]

Based on this computational evidence for conical intersections and on results from experimental studies, several deexcitation mechanisms have been proposed. The commonly accepted mechanism for adenine photorelaxation involves a fast $L_a \rightarrow n\pi^*$ transition followed by an $n\pi^* \rightarrow$ ground state transition.[2,4,11,13–15,27,28] Several groups have also reported a minimum-energy path directly connecting the optically active $\pi\pi^*$-L_a state to the ground state,[19,22–24,26] which should be responsible for the ultrafast decay component of the transient spectrum. Finally, the internal conversion from the L_a state to the ground state might also occur via the $\pi\sigma^*$ state (possibly involving a second transition to the $n\pi^*$ state), although this mechanism is believed to significantly contribute only at either low[13,17] or high[29] excitation energies. A schematic view of the deexcitation pathways is given in Figure 1.

Despite the large number of experimental and theoretical studies, the exact mechanism underlying the photodynamics of adenine is still not completely understood. In particular, further investigations are needed to determine the relative importance of individual deexcitation paths, as previous theoretical studies lack a dynamic treatment. After submission of this work, mixed quantum-classical dynamics simulations at the multireference configuration interaction (MR-CIS) level were reported for 9H-adenine,[30] following similar work on the aminopyrimidine model system.[31] These simulations identify a two-step deactivation process from the bright L_a state to the ground state, without evidence for a competing one-step process and without any major role of the $n\pi^*$ state.[30]

In this work, we report a surface-hopping study of the photodeexcitation dynamics of 9H-adenine (henceforth, adenine; Figure 2), the most abundant tautomer of adenine. Energies, gradients, and nonadiabatic couplings of the lowest excited states of adenine were calculated on the fly using the semiempirical OM2 method,[32,33] and hopping probabilities were evaluated by the fewest-switches algorithm.[34–36] The use of a direct approach

10.1021/jp8033402 CCC: $40.75
Published on Web 07/09/2008

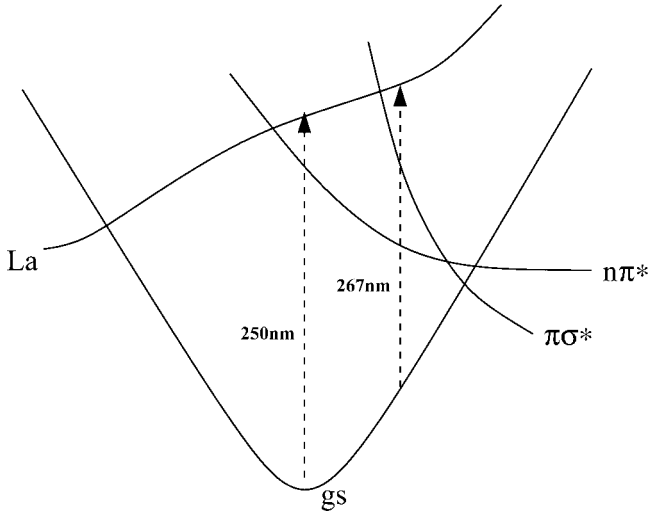

Figure 1. Schematic view of the possible deexcitation pathways of adenine. Arrows indicate the excitations from the ground state to the optically active $\pi\pi^*$-L_a state at different excitation wavelengths.

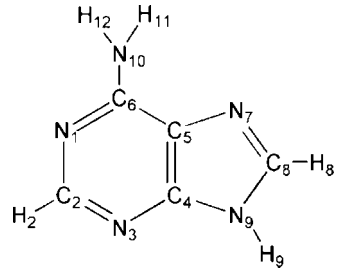

Figure 2. Structure and atom labeling for 9H-adenine.

allows the straightforward inclusion of all internal degrees of freedom with no need to make any preconceived assumption on the possible decay paths. The dynamics of the radiationless deactivation of adenine after vertical excitation into the optically active $\pi\pi^*$-L_a state can be followed in this manner, and the relative importance of individual contributions can be estimated. Moreover, a comparison with experimental time-resolved photoelectron spectroscopy results[13] is possible. The article is organized as follows: Section 2 outlines the methodology and specifies the computational details. In section 3, we report optimized geometries at critical points (energy minima and conical intersections), excitation energies at optimized geometries, and results of surface-hopping calculations. In section 4, we compare our results with experimental time-resolved photoelectron spectroscopy. Finally, conclusions are offered in section 5.

2. Computational Details

All calculations were performed using the semiempirical MNDO program.[37] Molecular orbitals were obtained using the orthogonalization-corrected OM2 semiempirical Hamiltonian.[32,33] Energies and gradients were calculated by the multireference GUGA-CI approach[38] using four reference configurations and an active space including 12 electrons in 10 orbitals.

The equilibrium geometries of the ground state and lowest excited state were optimized, and conical intersections connecting the lowest three states were located using a Lagrange−Newton method.[39,40] Vertical excitation energies were computed for the three lowest states of adenine in different geometrical configurations. Because the ordering of the states can change at different geometries, the excited states are labeled according to their electronic character ($n\pi^*$, $\pi\pi^*$-L_a, $\pi\pi^*$-L_b). In regions where the electronic character of a state cannot be defined (i.e., around conical intersections), the label indicates the state diabatically connected to the corresponding state.

TABLE 1: Excited-State Energies (eV) Relative to the Ground-State Minimum (gs)[a]

geometry	state	OM2	other methods
gs	$n\pi^*$	4.58 (0.00)	4.86 (0.00),[b] 4.96 (0.00)[c]
	L_a	4.66 (0.21)	4.97 (0.21),[b] 5.35 (0.18)[c]
	L_b	4.97 (0.14)	5.20 (0.01),[b] 5.16 (0.00)[c]
$(n\pi^*)_{min}$	gs	0.62 (−)	0.55 (−)[d]
	$n\pi^*$	4.11 (0.04)	3.85 (0.00)[d]
	L_b	4.97 (0.03)	4.57 (0.05)[d]
	L_a	5.05 (0.27)	4.59 (0.13) [d]

[a] Oscillator strengths are given in parentheses. [b] TD-DFT, ref 44. [c] CASPT2, ref 22. [d] DFT/MRCI, ref 19.

Nonadiabatic molecular dynamics simulations were performed using the recent MNDO surface-hopping implementation.[36] Trajectories were propagated for 1 ps with a time step of $dt = 0.2$ fs. The nonadiabatic coupling vectors were computed following the analytical procedure described in refs 40 and 41. The quantum amplitudes were propagated using a unitary propagator and a time step $dt' = dt/500$. The fewest-switches algorithm[34–36] was used to obtain hopping probabilities. Final results were obtained by averaging over 100 trajectories.

Only the lowest three states of adenine were included in the surface-hopping calculations, because the L_b state (fourth state at all relevant geometries) has only a marginal role in the deexcitation dynamics. This was confirmed by surface-hopping test calculations including all four states. Moreover, it should be noted that our calculations also exclude the $\pi\sigma^*$ state, which is of Rydberg type and cannot be correctly described by the semiempirical OM2 approach. This state plays an important role in the relaxation dynamics only for relatively high or low excitation energies, whereas it is not relevant for excitations with energies close to the vertical excitation energy.[13,17,29] For this reason, we selected the initial configurations for the surface-hopping calculations such that they sample only the center of the absorption band (see section 3.2), and the comparison with experimental results is restricted to measurements using an excitation wavelength of 250 nm.

3. Results

3.1. Potential Energy Surfaces. To characterize the potential energy surfaces of the lowest excited states of adenine, we optimized the most important geometrical configurations (energy minima and conical intersections) and computed the lowest excitation energies at each configuration.

Vertical excitation energies of adenine calculated at the equilibrium geometry of the ground state and $n\pi^*$ state are reported in Table 1. The optimized ground-state minimum geometry agrees well with previous ab initio results.[18,22,28] The most notable difference is that the molecule is completely planar in OM2, whereas the ab initio calculations yield a slight pyramidalization of the amino group that lowers the total energy by about 0.01 eV. The absence of small distortions in the OM2-optimized structure is probably due to the lack of polarization functions in the OM2 basis set.[28] At the optimized ground-state geometry, the three lowest excited singlet states are close in energy. In OM2, the lowest is the $n\pi^*$ state, followed by the $\pi\pi^*$-L_a and $\pi\pi^*$-L_b states. Both $\pi\pi^*$ states are optically active, with the L_a state showing the stronger optical coupling with the ground state, whereas the $n\pi^*$ state is computed to be a dark state.

The equilibrium geometry of the $n\pi^*$ state is characterized by a small pyramidalization of the amino group and an out-of-plane deformation of the six-membered ring described by the dihedral angle $\delta(C_6N_1C_2N_3) = 26°$. Similar structures were found at the ab initio level.[18,20,22] Going from the ground-state to the $n\pi^*$-state equilibrium geometry, the ground state is destabilized by 0.62 eV, whereas the $n\pi^*$ state is stabilized by 0.47 eV, and hence, the corresponding energy gap is reduced by 1.09 eV. The energy of the L_b state remains unchanged, whereas the L_a state is destabilized by 0.39 eV and thus lies slightly above the L_b state at the $n\pi^*$-state equilibrium geometry.

The OM2 excitation energies are in reasonable agreement with previous high-level calculations, although, because of the small energy gaps involved, the exact ordering of the low-lying excited states at the ground-state geometry is still not completely established and different methods yield different results. At the CASPT2 level, the lowest state is predicted to be of $n\pi^*$ character,[22–24] except in older studies where it was found at higher energies, probably because of the use of an incomplete active space for the CASSCF calculations.[18,20,42] The CASPT2 order of the two $\pi\pi^*$ states is $L_b < L_a$. At the TD-DFT level, the states are calculated in the same energy order as in OM2 ($n\pi^*$, L_a, L_b) but at higher energies.[21,25,43,44] In the case of DFT/MRCI, the $n\pi^*$ state is computed to have an energy intermediate between those of the L_b state (lowest energy) and the L_a state (highest energy).[19]

It should be noted, however, that the precise order of the low-lying excited states at the ground-state minimum geometry of adenine is less essential for the description of the nonadiabatic dynamics than one might initially expect. This order changes with molecular geometry during the dynamics, and more importantly, the excited states rapidly acquire a mixed character after the vertical excitation because the dynamics proceeds through the conical intersection connecting the L_a and $n\pi^*$ states [$(L_a/n\pi^*)_{CI}$]. Therefore, the relaxation dynamics is not highly sensitive to the original state ordering. Finally, on the basis of experimental results,[13,17] the L_b state is not believed to play a role in the deexcitation process, and indeed, all theoretical methods predict a destabilization of the L_b state in distorted geometries.

No OM2 equilibrium geometry could be found for the L_a state, because energy minimizations starting from the ground-state geometry led directly to the conical intersection connecting the L_a and the ground state [$(L_a/gs)_{CI}$]. This finding is compatible with the existence of a barrierless descending path linking the Franck−Condon region with the conical intersection that has already been described at the CASSCF level.[22–24] However, to understand the photophysics of adenine, it is important to note that this minimal-energy path also crosses the $n\pi^*$ potential energy surface.

The $(L_a/n\pi^*)_{CI}$ conical intersection is characterized by out-of-plane distortions. The six- and five-membered rings do not lie in the same plane but form an angle of ∼15°. In the six-membered ring, there is an out-of-plane deformation of the $N_1{-}C_2H_2{-}N_3$ moiety and a small pyramidalization of the amino group. In this configuration, the ground state is destabilized by 0.7 eV, whereas the lowest excited states are only slightly stabilized, so that the resulting energy gap is 3.7 eV (see Figure 3).

At the $(L_a/gs)_{CI}$ conical intersection, strong out-of-plane deformations are observed, in particular at the C_2 atom. The computed dihedral angles are $\delta(C_6N_1C_2N_3) = 68.4°$ and $\delta(C_6N_1C_2H_2) = -82.6°$, which compare well with previous CASSCF calculations yielding $\delta(C_6N_1C_2N_3) = 67.6°$ [18] and $\delta(C_6N_1C_2H_2) = -82.6/-94.7°$.[18,22] In this geometry, the ground-state energy is 4 eV higher than in the ground-state equilibrium configuration, and the energy of the lowest excited state (L_a) is slightly reduced. By contrast, the energies of other excited states are raised in this configuration.

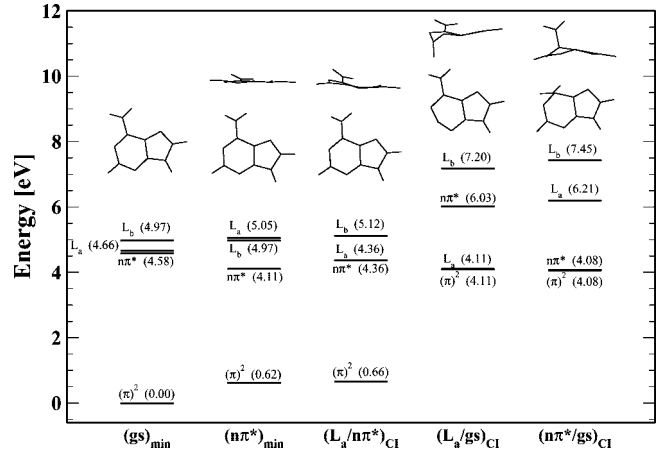

Figure 3. OM2 energies of the low-lying states of adenine calculated at different nuclear configurations (energies relative to the ground-state minimum given in parentheses). At the top are the structures corresponding to the configurations.

Finally, a conical intersection connecting the $n\pi^*$ and ground states [$(n\pi^*/gs)_{CI}$] can be located. It is characterized by a strong out-of-plane bending of the amino group and an out-of plane deformation of the $N_1{-}C_2H_2{-}N_3$ moiety. The respective dihedral angles are $\delta(C_2N_1C_6N_6) = 71.8°$ and $\delta(C_6N_1C_2H_2) = -162.9°$ at the OM2 level. These results compare well with CASSCF findings of $\delta(C_2N_1C_6N_6) \approx 66°$ [18,22] and $\delta(C_6N_1C_2H_2) = -142.3°$.[18] The strong deformations characterizing the $(n\pi^*/gs)_{CI}$ conical intersection cause a small lowering of the energy of the lowest excited state ($n\pi^*$) and a strong increase of the energy of the ground state and the higher excited states.

The OM2 energies and geometries are summarized in Figure 3. Overall, they agree well with previous ab initio[18,20,22–24,27,43] and density functional[19,21,43] calculations. (See Tables 1 and 2.)

TABLE 2: Energies (eV) of the $n\pi^*$ Minimum and the Indicated Conical Intersections[a] Relative to the Ground-State Minimum

structure	OM2	other results
$(n\pi^*)_{min}$	4.11	4.35,[b] 4.48,[c] 4.40[d]
$(L_a/n\pi^*)_{CI}$	4.36	
$(L_a/gs)_{CI}$	4.11	4.06,[b] 4.17,[c] 4.09[e]
$(n\pi^*/gs)_{CI}$	4.08	4.55,[b] 4.12[c]

[a] See text. [b] CASPT2, ref 24. [c] CASPT2, ref 18. [d] Experimental, ref 6. [e] CASPT2, ref 22.

3.2. Surface-Hopping Dynamics. Surface-hopping calculations on 100 trajectories were performed to follow the nonadiabatic dynamics of adenine after vertical excitation into the L_a state (second excited state, S_2). The starting configurations were selected in order to approximately sample the center of the absorption band by taking 20 snapshots at regular intervals of 250 fs from a ground-state molecular dynamics simulation. Each chosen configuration was then used as a starting point for several surface-hopping trajectories, with the number of trajectories proportional to the oscillator strength of the starting configuration. The corresponding absorption spectrum is reported in Figure 4. It agrees well with the experimental

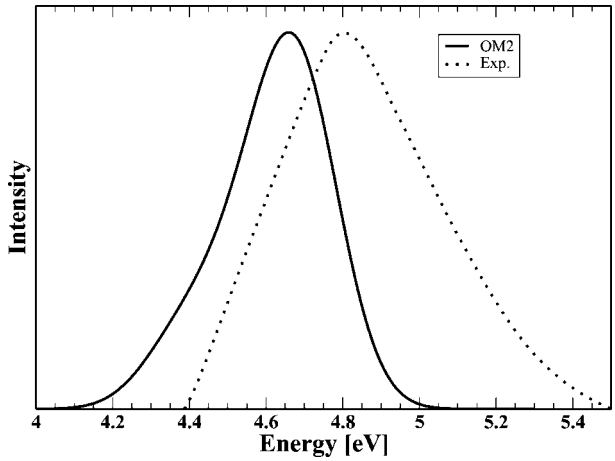

Figure 4. OM2-computed absorption spectrum defining the initial conditions for the surface-hopping simulation. The experimental absorption spectrum from ref 1 is shown as dotted line.

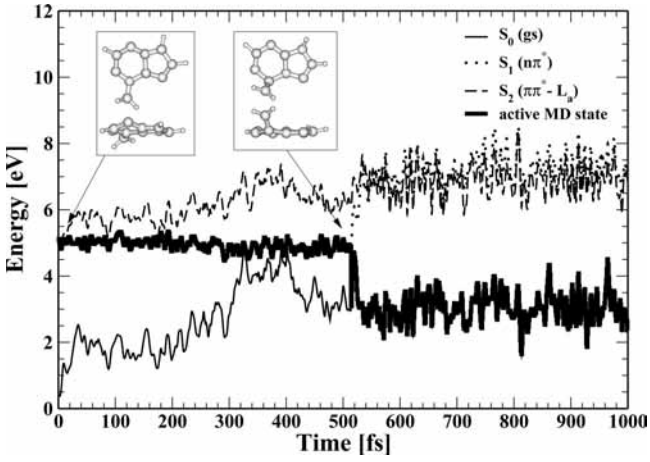

Figure 5. Potential energy surfaces for a typical trajectory following the $(n\pi^*/\mathrm{gs})_{\mathrm{CI}}$ decay path.

spectrum,[1,6] except for a small red shift (~0.15 eV) and the neglect of any contribution from the L_b state in the computed spectrum that makes it narrower at higher energies.

All trajectories start in the S_2 (L_a) state. The molecule immediately begins to follow the downhill path toward the $(L_a/\mathrm{gs})_{\mathrm{CI}}$ conical intersection, characterized by out-of-plane deformations. However, along this path, about 10−40 fs after the beginning of the dynamics, the $(L_a/n\pi^*)_{\mathrm{CI}}$ conical intersection is reached. Here, the molecule has a strongly mixed character, oscillating between $\pi\pi^*$-L_a and $n\pi^*$, and hopping to the S_1 surface (with $n\pi^*$ character) is highly probable. The dynamics then follows the S_1 potential energy surface, evolving toward the $(n\pi^*/\mathrm{gs})_{\mathrm{CI}}$ conical intersection. The molecule oscillates several times around this configuration until it finally hops to the ground state. A typical trajectory following this path is shown in Figure 5.

A small number of trajectories (~10%) follow a different deexcitation path. In this case, after the hop to the S_1 surface the $\pi\pi^*$-L_a character is retained, possibly because the molecule does not quite reach the $(L_a/n\pi^*)_{\mathrm{CI}}$ conical intersection. The dynamics proceeds on the S_1 potential energy surface (with L_a character) until the $(L_a/\mathrm{gs})_{\mathrm{CI}}$ conical intersection is reached (usually within 100−300 fs). Here, hopping directly to the ground state occurs. This situation is depicted in Figure 6 for a typical trajectory.

The nonadiabatic dynamics can also be analyzed in terms of the relative contribution to the total populations from states with

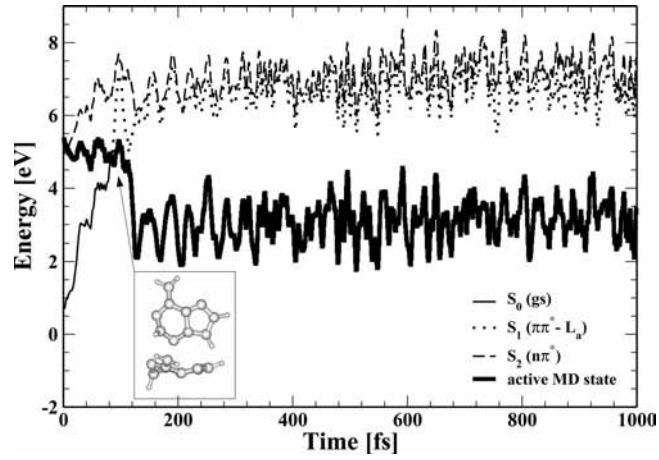

Figure 6. Potential energy surfaces for a typical trajectory following the $(L_a/\mathrm{gs})_{\mathrm{CI}}$ decay path.

different electronic characters. The relative population of each state as a function of time can be fitted using the equations

$$p(t) = \mathrm{e}^{-t/\tau_{\mathrm{L_a}}} \quad \text{for the } \mathrm{L_a} \text{ state} \tag{1}$$

$$p(t) = \frac{\tau_{n\pi^*}}{\tau_{\mathrm{L_a}} - \tau_{n\pi^*}}[\mathrm{e}^{-t/\tau_{\mathrm{L_a}}} - \mathrm{e}^{-t/\tau_{n\pi^*}}] \quad \text{for the } n\pi^* \text{ state} \tag{2}$$

where the time constants are $\tau_{\mathrm{L_a}} = 15$ fs and $\tau_{n\pi^*} = 560$ fs. The population of states exhibiting L_a character shows an ultrafast decay, mainly due to the motion through the $(L_a/n\pi^*)_{\mathrm{CI}}$ conical intersection, which occurs within 10−50 fs, with a smaller contribution from the second channel proceeding through the $(L_a/\mathrm{gs})_{\mathrm{CI}}$ conical intersection, which has the effect of slightly increasing the decay time. The ultrafast transfer of population from L_a to $n\pi^*$ is also responsible for the extremely quick increase of the population of states with $n\pi^*$ character, which reaches a maximum around $t \approx 30-40$ fs. After this time, there is no more transfer of population from L_a, and the $n\pi^*$ population shows a slow exponential decay.

4. Comparison with Experimental Results

Results from surface-hopping calculations can be compared with time-resolved photoelectron spectroscopy results.[13] In our calculations, the initial conditions were generated by sampling the center of the absorption band of adenine, so that we can compare with measurements performed using a pump wavelength of 250 nm. However, care is needed to account for differences in the excitation process. In surface-hopping calculations, the excitation is assumed to be instantaneous, and the time $t = 0$ is set for all trajectories exactly at the time of the instantaneous excitation. This corresponds to an excitation from a laser with infinitesimal time width. However, in the experimental setup, a laser pulse with a finite time width is used, which results in a slightly different deexcitation dynamics.

To a first approximation, the measured signal for a given state will correspond to the convolution of the laser pulse and the occupation of this state as a function of time. Assuming a simple Gaussian shape for the laser pulse, the intensity, P, of the signal is thus given by

$$P(t) = \int \mathrm{d}\tau\, \mathrm{e}^{-\alpha(\tau-\tau_0)^2} p(t-\tau) \tag{3}$$

where p is determined from the surface-hopping calculations (eq 1 or 2).

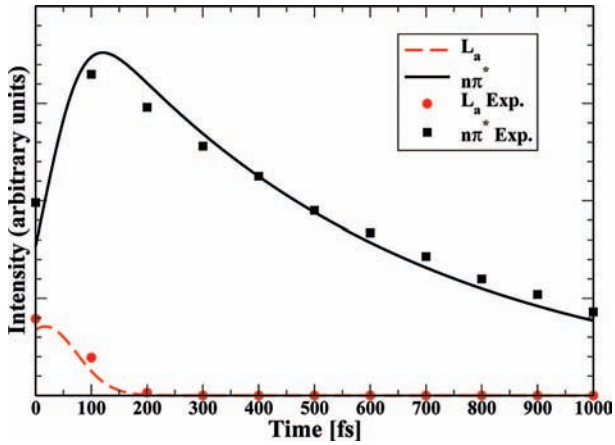

Figure 7. Relative populations of excited states of $\pi\pi^*$-L_a and $n\pi^*$ character as function of time after excitation with a laser pulse of finite duration. Experimental data are from ref 13.

For the laser parameters, we used $\tau_0 = 0$ fs and $\alpha = 2.8 \times 10^{-4}$ fs^{-2}; that is, we considered a laser pulse centered on the time origin with a full width at half-maximum of 100 fs. The resulting plots for states of L_a and $n\pi^*$ character are shown in Figure 7. The two curves agree well with experimental data (denoted by circles and squares) both in relative intensity and in decay behavior. The computed decay times of the two states are $\tau_{L_a} = 45$ fs and $\tau_{n\pi^*} = 570$ fs, which agree well with measured values of $\tau_{L_a} = 50$ fs and $\tau_{n\pi^*} = 750$ fs.

5. Conclusions

We have studied the nonradiative deexcitation dynamics of 9H-adenine by means of surface-hopping simulations using OM2 potential energy surfaces. Before carrying out the dynamic study, we characterized the potential energy surfaces of the lowest electronic states by performing geometry optimizations of the critical points (energy minima and conical intersections) and computing excitation energies. The corresponding OM2 results are in reasonable agreement with the available ab initio and density functional results.

Surface-hopping calculations were performed to simulate the nonadiabatic dynamics of adenine excited at energies close to the center of the absorption band. We find that the system relaxes to the ground state through a two-step process characterized by an ultrashort $S_2 \rightarrow S_1$ transition followed by a $S_1 \rightarrow S_0$ transition. Most trajectories follow the deexcitation path through the $(n\pi^*/gs)_{CI}$ conical intersection, and only a minor contribution is made by trajectories proceeding through the $(L_a/gs)_{CI}$ conical intersection.

An analysis of the relative population of the excited states with different electronic characters (L_a or $n\pi^*$) reveals a distinctly different decay behavior. The number of states with L_a character decreases rapidly with an exponential decay time of 15 fs. The number of states with $n\pi^*$ character shows instead a slower decay with a time constant of 560 fs. These findings are fully compatible with experimental time-resolved photodetachment photoelectron spectroscopy.

Acknowledgment. We thank Zhenggang Lan (MPI Mülheim) for helpful discussions. This work was supported by the Deutsche Forschungsgemeinschaft (SFB 663).

References and Notes

(1) Callis, P. R. *Annu. Rev. Phys. Chem.* **1983**, *34*, 329.
(2) Crespo-Hernandez, C. E.; Cohen, B.; Hare, P. M.; Kohler, B. *Chem. Rev.* **2004**, *104*, 1977.
(3) Crespo-Hernandez, C. E.; Cohen, B.; Kohler, B. *Nature* **2005**, *436*, 1141.
(4) Saigusa, H. *J. Photochem. Photobiol. C* **2006**, *7*, 197.
(5) Shukla, M. K.; Leszczynski, J. *J. Biomol. Struct. Dyn.* **2007**, *25*, 93.
(6) Kim, N. J.; Jeong, G.; Kim, Y. S.; Sung, J.; Kim, S. K.; Park, Y. D. *J. Chem. Phys.* **2000**, *113*, 10051.
(7) Clark, L. B.; Tinoco, I. *J. Am. Chem. Soc.* **1965**, *87*, 11.
(8) Voelter, W.; Records, R.; Bunnenberg, E.; Djerassi, C. *J. Am. Chem. Soc.* **1968**, *90*, 6163.
(9) Fucaloro, A.; Forster, L. S. *J. Am. Chem. Soc.* **1971**, *93*, 1378.
(10) Kang, H.; Jung, B.; Kim, S. K. *J. Chem. Phys.* **2003**, *118*, 6717.
(11) Kang, H.; Lee, K. T.; Jung, B.; Ko, Y. J.; Kim, S. K. *J. Am. Chem. Soc.* **2002**, *124*, 12958.
(12) Ullrich, S.; Shultz, T.; Zgierski, M. Z.; Stolow, A. *Phys. Chem. Chem. Phys.* **2004**, *6*, 2796.
(13) Ullrich, S.; Shultz, T.; Zgierski, M. Z.; Stolow, A. *J. Am. Chem. Soc.* **2004**, *126*, 2262.
(14) Canuel, C.; Mons, M.; Piuzzi, F.; Tardivel, B.; Dimicoli, I.; Elhanine, M. *J. Chem. Phys.* **2005**, *122*, 074316.
(15) Samoylova, E.; Lippert, H.; Ullrich, S.; Hertel, I. V.; Radloff, W.; Shultz, T. *J. Am. Chem. Soc.* **2005**, *127*, 1782.
(16) Ritze, H.-H.; Lippert, H.; Samoylova, E.; Smith, V. R.; Hertel, I. V.; Radloff, W.; Shultz, T. *J. Chem. Phys.* **2005**, *122*, 224320.
(17) Satger, H.; Townsend, D.; Zgierski, M.; Patchkovskii, S.; Ullrich, S.; Stolow, A. *Proc. Natl. Acad. Sci. U.S.A.* **2006**, *103*, 10196.
(18) Perun, S.; Sobolewski, A. L.; Domcke, W. *J. Am. Chem. Soc.* **2005**, *127*, 6257.
(19) Marian, C. M. *J. Chem. Phys.* **2005**, *122*, 104314.
(20) Chen, H.; Li, S. *J. Phys. Chem. A* **2005**, *109*, 8443.
(21) Nielsen, S. B.; Sølling, T. I. *ChemPhysChem* **2005**, *6*, 1276.
(22) Serrano-Andrès, L.; Merchàn, M.; Borin, A. C. *Chem. Eur. J.* **2006**, *12*, 6559.
(23) Serrano-Andrès, L.; Merchàn, M.; Borin, A. C. *Proc. Natl. Acad. Sci. U.S.A.* **2006**, *103*, 8691.
(24) Blancafort, L. *J. Am. Chem. Soc.* **2006**, *128*, 210.
(25) Sobolewski, A. L.; Domcke, W. *Eur. J. Phys. D* **2002**, *20*, 369.
(26) Perun, S.; Sobolewski, A. L.; Domcke, W. *Chem. Phys.* **2005**, *313*, 107.
(27) Zgierski, M. Z.; Patchkovskii, S.; Lim, E. C. *Can. J. Chem.* **2007**, *85*, 124.
(28) Broo, A. *J. Phys. Chem. A* **1998**, *102*, 526.
(29) Nix, M. G. D.; Devine, A. L.; Cronin, B.; Ashfold, M. N. R. *J. Chem. Phys.* **2007**, *126*, 124312.
(30) Barbatti, M.; Lischka, H. *J. Am. Chem. Soc.* **2008**, *130*, 6831.
(31) Barbatti, M.; Lischka, H. *J. Phys. Chem. A* **2007**, *111*, 2852.
(32) Weber, W. Ph.D. Thesis, Universität Zürich, Zürich, Switzerland, 1996.
(33) Weber, W.; Thiel, W. *Theor. Chem. Acc.* **2000**, *103*, 495.
(34) Tully, J. C. *J. Chem. Phys.* **1990**, *93*, 1061.
(35) Hammes-Schiffer, S.; Tully, J. C. *J. Chem. Phys.* **1994**, *101*, 4657.
(36) Fabiano, E.; Keal, T. W.; Thiel, W. *Chem. Phys.* **2008**, *349*, 334.
(37) Thiel, W. *MNDO Program*, version 6.1; Max-Planck-Institut für Kohlenforschung, Mülheim an der Ruhr, Germany, 2007.
(38) Koslowski, A.; Beck, M. E.; Thiel, W. *J. Comput. Chem.* **2003**, *24*, 714.
(39) Manaa, M. R.; Yarkony, D. R. *J. Chem. Phys.* **1993**, *99*, 5251.
(40) Keal, T. W.; Koslowski, A.; Thiel, W. *Theor. Chem. Acc.* **2007**, *118*, 837.
(41) Lengsfield III, B. H.; Yarkony, D. R. *Adv. Chem. Phys.* **1992**, *82*, 1.
(42) Fülscher, M. P.; Serrano-Andrès, L.; Ross, B. O. *J. Am. Chem. Soc.* **1997**, *119*, 6168.
(43) Mennucci, B.; Toniolo, A.; Tomasi, J. *J. Phys. Chem. A* **2001**, *105*, 4749.
(44) Shukla, M. K.; Leszczynski, J. *J. Comput. Chem.* **2004**, *25*, 768.

JP8033402